EFFECT OF PROCESS PARAMETERS ON THE PREPARATION OF *C@ZrSiO₄* BY PFA-NHSG METHOD

Junxiong ZHANG[1], Feng JIANG[*,1], Wen LI[1], Guo FENG[1], Quan ZHANG[1], Xiaojun ZHANG[2], Jianmin LIU[2], Guirong XU[2], Zhiyuan LI[3]

Inorganic black ceramic pigments, particularly spinel-structured systems (e.g., Fe–Cr–Ni–Mn), face critical limitations due to toxic metal content and chromatic instability in zinc/barium-rich glazes. While carbon black offers a low-cost, eco-friendly alternative, its susceptibility to oxidation at high temperatures necessitates robust encapsulation strategies. Zirconium silicate ($ZrSiO_4$) has emerged as a promising encapsulant, yet conventional synthesis methods often yield incomplete carbon coverage and suboptimal chromaticity. To address these challenges, this study developed a pressure field-assisted non-hydrolytic sol-gel (PFA-NHSG) method to synthesize C@$ZrSiO_4$ pigments with a novel seed-pulp structure. Using zirconium butoxide and in situ carbon precursors, the effects of non-hydrolytic reaction temperature (140–180°C), pressure field duration (8–20 h), and calcination conditions (875–950°C) were systematically optimized. Key findings reveal that 170°C, 12 h pressure treatment, and 925°C calcination yield dense $ZrSiO_4$ shells encapsulating uniformly dispersed in situ carbon nanoparticles (~20 nm), achieving optimal chromaticity (L = 21.32). Mechanistic analyses demonstrate that pressure fields enhance Si–O–Zr bond formation while directing carbon precursor reorganization into C=C bonds, suppressing etherification and improving carbon retention. The pigments exhibit exceptional high-temperature stability (1200°C) in glazes, retaining structural integrity and uniform coloration. This work provides an eco-friendly strategy for designing durable ceramic pigments through synergistic control of inorganic crystallization and carbon precursor carbonization.*

Keywords: C@$ZrSiO_4$, non-hydrolytic sol-gel, pressure field, pigment

1. Introduction

Inorganic black pigments are among the most extensively utilized decorative materials due to their pure, dignified, and elegant visual effects. They hold significant industrial applications in glaze formulations, ceramic bodies, sanitary ware, tiles, inkjet printing, and related fields [1~4]. Currently, commercially prevalent black ceramic pigments predominantly adopt spinel-structured systems such as Fe-Cr-Ni-Mn and Fe-Cr-Co-Ni [5, 6]. Despite their widespread adoption, spinel-based black pigments exhibit non-negligible

[1] School of Material Science and Engineering, Jingdezhen Ceramic University, Jingdezhen, Jiangxi, China, Corresponding author: jiangfeng@jci.edu.cn
[2] National Engineering Research Center for Domestic and Building Ceramics, Jingdezhen, Jiangxi, China
[3] Jingdezhen Vocational University of Art, Jingdezhen, Jiangxi, China

limitations: (1) inherent toxicity from hazardous metal constituents poses risks to human health and ecosystems; (2) chromatic aberrations frequently occur due to interactions with zinc or barium ions in base glazes [7].

Developing cost-effective and environmentally benign black pigments is imperative for advancing green manufacturing in the ceramics industry. Carbon black has garnered attention as a promising alternative owing to its accessibility and low cost. However, its susceptibility to oxidation under high-temperature calcination severely restricts practical applications in ceramic glazes. To address this challenge, zirconium silicate ($ZrSiO_4$)—a material renowned for its high transparency and exceptional thermochemical stability [8~10]—has been employed as an encapsulating matrix to protect carbon black from oxidative degradation.

For instance, Zhang et al. synthesized C@SiO_2@$ZrSiO_4$ pigments via layer-by-layer self-assembly, achieving remarkable high-temperature stability through a multilayered encapsulation architecture [11]. Nevertheless, structural randomness in the encapsulation layers often leads to incomplete carbon coverage, resulting in undesirable grayish hues. To optimize chromatic performance, homogeneous dispersion of carbon black in precursor solutions is critical. Agglomeration of carbon particles during synthesis may reduce both encapsulation efficiency and color intensity of C@$ZrSiO_4$ pigments. Post-calcination grayscale discoloration indicates oxidative loss of unprotected carbon.

Our research group has pioneered non-hydrolytic sol-gel methodologies for C@$ZrSiO_4$ pigment fabrication. Chen et al. demonstrated cotton fiber-derived carbon sources to synthesize C@$ZrSiO_4$ pigments ($L^* = 39.09$) with structural advantages [12]. Tang et al. achieved superior chromaticity ($L = 21.20$) through the in-situ carbonization of organic precursors, eliminating the need for external carbon sources. Additionally, they demonstrated that the incorporation of NAA reduces the synthesis temperature of the $ZrSiO_4$ phase to 850°C. Moreover, NAA enhances the dissolution of LiF in $C_4H_{10}O$ via coordination, thereby improving the mineralization effect and facilitating the formation of a dense $ZrSiO_4$ encapsulation structure. [13]. Jiang et al. further developed a pressure-assisted non-hydrolytic sol-gel route to produce seed-pulp structured C@$ZrSiO_4$ pigments, featuring carbon cores encapsulated within zirconium silicate shells [14]. Building upon these advancements, this work systematically investigates the effects of non-hydrolytic reaction time (4–20 h), temperature (140–180 ℃), and calcination parameters (875–950℃ for 2–4 h) on pigment synthesis via the pressure-assisted sol-gel method.

2. Experimental

2.1 Materials synthesis

Zirconium (IV) butoxide ($C_{16}H_{36}O_4Zr$, Shanghai Aladdin Biochemical Technology Co., AR, 99.0 %) and tetraethyl orthosilicate (TEOS, Xilong Chemical Co., AR, 99.0 %) served as zirconium and silicon sources, respectively. Lithium

fluoride (LiF, Shanghai Aladdin Biochemical Technology Co., AR, 99.0 %) and acetic acid ($C_2H_4O_2$, Shanghai Aladdin Biochemical Technology Co., > 99.8%) were employed as mineralization agent and additive. Carbon-containing organic groups acted as in situ carbon precursors, with n-butanol ($C_4H_{10}O$, > 99.0%, Sinopharm Chemical Reagent Co.) as solvent.

A precursor solution was prepared by mixing 0.12 mol TEOS (27 mL), 0.0035 mol LiF (0.091 g), and 0.03 mol $C_2H_4O_2$ (1.7 mL) in 50 mL n-butanol under 30-min stirring. Subsequently, 0.012 mol (4.39 mL) zirconium butoxide was introduced, followed by 4-h stirring at 60 ℃. The homogeneous mixture (around 83 mL 0.87 g/mL) was transferred to an autoclave (Volume: 100mL) and hydrothermally treated at 170 ℃ for 12 h to obtain a transparent precursor gel. The resultant gel was dried at 110 ℃ for 16 h to obtain xerogel powder. Finally, the prepared precursor gel was dried at 110°C for 16 hours to obtain a dry gel powder. This dry gel powder was then placed in a crucible, sealed with carbon powder, and subjected to heat treatment at 925°C for 3.5 hours. Subsequently, the carbon powder was removed, and the resulting product was maintained in air at 700°C for 2 hours to yield C@ZrSiO4, a black pigment exhibiting excellent coloring performance.

2.2. Characterization

X-ray diffraction (XRD): Phase analysis was conducted using a Bruker D8-Advance diffractometer (Cu-Kα radiation, λ = 0.15418 nm) with 2θ range 10°–70° at 0.02° step size and 10 s/step.

Electron microscopy: Microstructural evaluation utilized a Phenom Pro SEM (Netherlands) and Hitachi SU8010 FE-SEM. TEM/HRTEM/SAED/EDS analyses were performed on JEOL JEM-2010 and JEM-F200 instruments.

Chromaticity: Color coordinates (L*, a*, b*) were quantified via a WSD-3C whiteness meter (Beijing Kangguang Instrument Co.), adhering to CIE standards.

Infrared spectroscopy: The analysis was performed using a Nicolet 5700 FT-IR spectrometer (Thermo Fisher Scientific, USA). Measurements were conducted over a wavenumber range of 400 to 2000 cm^{-1} with a precision of 1.0 cm^{-1} to identify chemical bonds and functional groups in the samples.

3. Results and Discussion

3.1 Influence of Non-Hydrolytic Reaction Temperature on Pigment Synthesis

The reaction temperature in non-hydrolytic systems critically governs reaction kinetics, making its optimization pivotal for C@$ZrSiO_4$ pigment synthesis. Precursors were prepared at 140 ℃, 150 ℃, 160 ℃, 170 ℃, and 180 ℃ under 8 h isothermal conditions, followed by calcination at 900 ℃ (4 h) and 700 ℃ (2 h) in a protective atmosphere.

Fig. 1(a) displays XRD patterns of samples synthesized at varying temperatures. At 140 ℃, t-ZrO_2 (JCPDS #80-0784) dominates as the primary phase, with no detectable $ZrSiO_4$ diffraction, speculating insufficient reaction conditions due to inadequate pressure field intensity for Si-O-Zr ($ZrSiO_4$) bond formation [15]. Raising the temperature to 150 ℃ yields $ZrSiO_4$ (JCPDS #06-0266) as the main phase, albeit with weak crystallinity. Peak intensities progressively strengthen with increasing temperature, reaching optimal crystallinity at 170 ℃. Further elevation to 180 ℃ destabilizes Si-O-Zr bonding due to excessive pressure, impairing $ZrSiO_4$ crystallization.

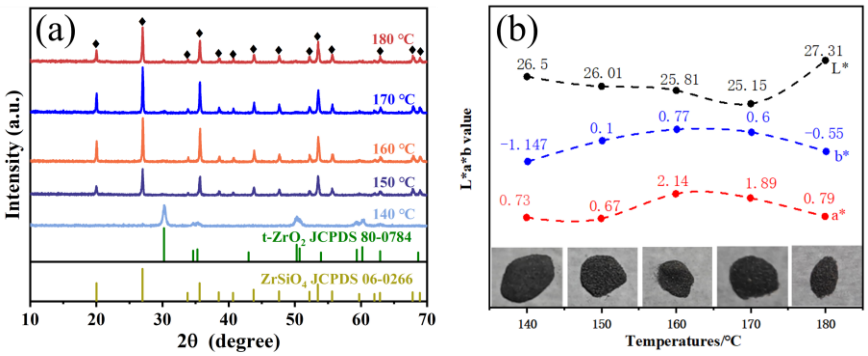

Fig. 1. XRD spectra (a) and coordinate curves of L*, a*, and b* values (b) of C@ZrSiO4 pigments prepared at different non-hydrolysis reaction temperatures

Fig. 1(b) illustrates chromatic coordinates (L*, a*, b*) of the pigments. The L* value initially decreases, reaching a minimum of 25.15 at 170 ℃ (deepest black hue), then increases at higher temperatures. Suboptimal temperatures (<170 ℃) yield poorly crystallized $ZrSiO_4$ with porous encapsulation, enabling partial carbon oxidation. Conversely, excessive pressure at >170 ℃ disrupts Si-O-Zr bonding, reducing encapsulation density and elevating L*. Notably, a* and b* values remain near zero, confirming neutral chromaticity. Thus, 170 ℃ was selected as the optimal reaction temperature.

Fig. 2 presents SEM images of samples synthesized at different temperatures. Based on the XRD results presented in Fig. 1, it is evident that at 140°C, Zr-O-Zr (t-ZrO_2) bonding predominates. [16], while Si-O-Zr ($ZrSiO_4$) bonds emerge at 150 ℃. Progressive temperature increases enhance $ZrSiO_4$ crystallinity, forming dense, stacked particles at 170 ℃. At 180 ℃, heterogeneous and fragmented $ZrSiO_4$ grains arise due to pressure-induced structural instability.

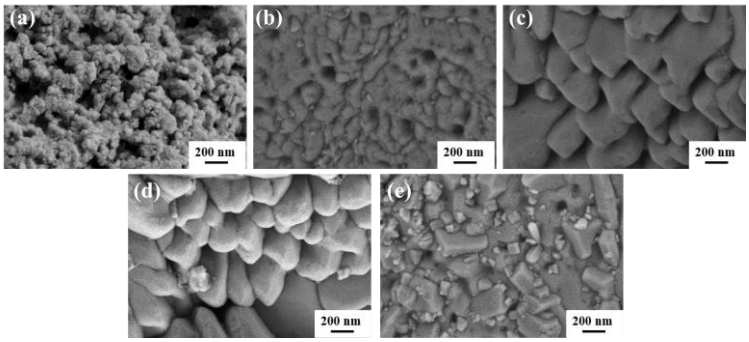

Fig. 2. SEM images of C@ZrSiO4 pigments prepared at different hydrothermal temperatures: 140(a); 150(b); 160(c); 170(d); 180(e)

3.2 Effect of Pressure Field Duration on Synthesis

In non-hydrolytic reactions, the duration of pressure field treatment significantly modulates reaction kinetics, making its optimization critical for synthesizing C@ZrSiO₄ pigments. To systematically evaluate this parameter, precursors were prepared under a fixed Si/Zr molar ratio of 1.2:1 and a non-hydrolytic reaction temperature of 170 ℃, with pressure field exposure times of 8 h, 12 h, 16 h, and 20 h. The resulting precursors were calcined at 900 ℃ for 4 h under a protective atmosphere, followed by oxidation at 700 ℃ for 2 h to obtain final pigments.

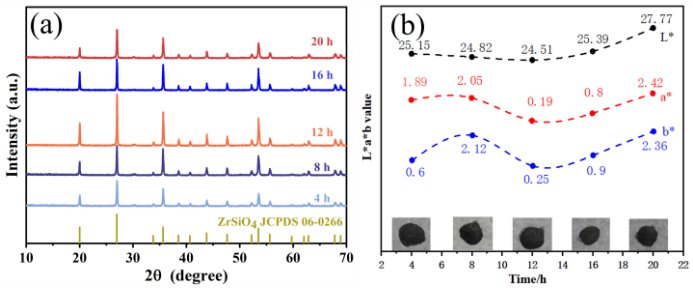

Fig. 3. XRD spectra (a) and coordinate curves of L*, a*, and b* values (b) of C@ZrSiO4 pigment prepared with different pressure field treatment times

Fig. 3(a) presents XRD patterns of samples subjected to varying pressure field durations. All patterns exhibit pure-phase ZrSiO₄ diffraction peaks (JCPDS #06-0266), with no detectable impurity phases. Notably, ZrSiO₄ crystallinity initially improves with increasing treatment time, reaching maximum intensity at 12 h, then declines upon further prolongation. This trend indicates that moderate pressure field exposure enhances crystallization, whereas excessive duration destabilizes the system. Fig. 3(b) illustrates chromatic coordinates (L*, a*, b*) of the synthesized pigments. The L* value decreases progressively, attaining a

minimum of 24.51 at 12 h, corresponding to optimal black chromaticity. Beyond 12 h, L* values rise, reflecting diminished color quality.

Fig. 4 displays SEM microstructures of samples processed at different durations. At 12 h, $ZrSiO_4$ particles exhibit well-packed morphology with negligible intergranular porosity, signifying high crystallinity and dense encapsulation. Shorter durations (8 h) yield porous structures due to incomplete polycondensation, which weakens Si-O-Zr bonding [15]. Conversely, prolonged treatment (>12 h) induces mechanical degradation of performed Si-O-Zr networks under sustained pressure, leading to fragmented and irregular grains. The pressure field facilitates polycondensation by promoting covalent Si-O-Zr bond formation. At 12 h, equilibrium between bond formation and structural stabilization is achieved, maximizing crystallinity. Insufficient exposure (<12 h) limits reaction completeness, while overexposure (>12 h) introduces shear stresses that disrupt existing bonds. These findings underscore the necessity of balancing pressure field duration to optimize both structural integrity and chromatic performance.

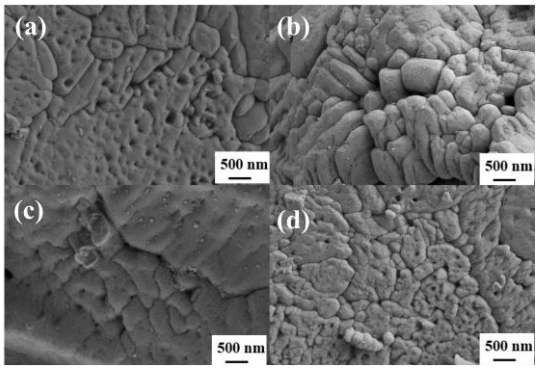

Fig. 4. SEM pattern of C@ZrSiO4 pigment prepared with different pressure field treatment times : 8 h(a); 12 h(b); 16 h(c); 20 h(d)

3.3 Influence of Heat Treatment Temperature on Pigment Synthesis

Fig. 5(a) displays XRD patterns of $C@ZrSiO_4$ pigments synthesized at varying calcination temperatures (875 ℃, 900 ℃, 925 ℃, and 950 ℃). All patterns confirm the successful formation of pure-phase $ZrSiO_4$ crystals (JCPDS #06-0266). The diffraction peak intensities progressively strengthen with increasing temperature, indicating enhanced crystallinity. This trend arises because elevated thermal energy promotes atomic rearrangement and crystallization during $ZrSiO_4$ growth.

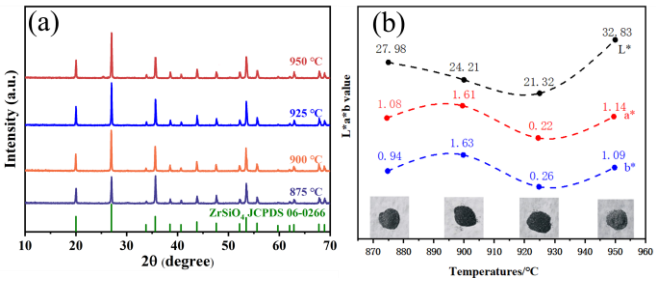

Fig. 5. XRD spectra (a) and coordinate curves of L*, a*, and b* values (b) of C@ZrSiO4 pigment prepared with different heat treatment temperatures

Fig. 5(b) illustrates the chromatic coordinates (L*, a*, b*) of the pigments. The L* value initially decreases, reaching a minimum of 21.32 at 925 ℃ (optimal blackness), then increases at higher temperatures. This non-monotonic behavior reflects a balance between encapsulation quality and carbon retention.

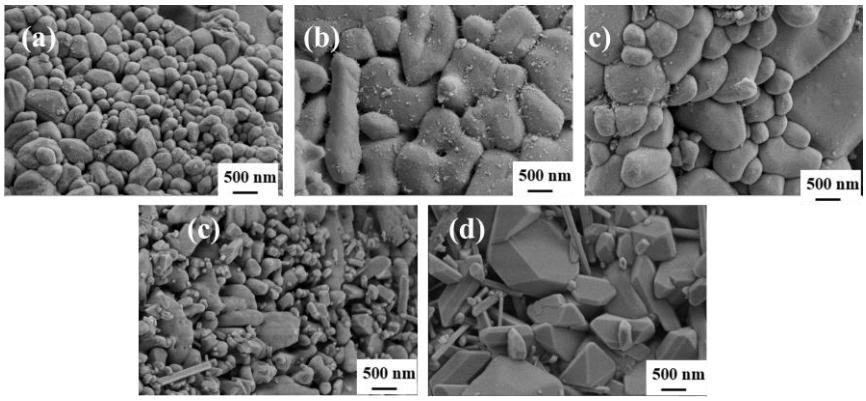

Fig. 6. SEM patterns of C@ZrSiO4 pigment prepared with different heat treatment temperatures: 875(a); 900(b); 925(c); 950(d); 975(e)

Fig. 6 presents SEM microstructures of samples calcined at different temperatures. Below 925 ℃ (e.g., 875–900 ℃), incomplete crystallization results in porous $ZrSiO_4$ shells (Figs. 6b), which inadequately protect the carbon cores from oxidation. At 925 ℃ (Fig. 6c), dense and homogeneous $ZrSiO_4$ coatings form, ensuring complete carbon encapsulation. However, exceeding 925 ℃ (e.g., 950 ℃, Fig. 6d) induces overgrowth of $ZrSiO_4$ crystals, leading to excessively thick shells and partial carbon exposure due to localized $ZrSiO_4$ crystallization independent of the carbon cores. Additionally, elongated $ZrSiO_4$ grains emerge at higher temperatures, accompanied by oversized particles due to excessive densification. Thus, 925 ℃ was identified as the optimal calcination temperature.

3.4 High-Temperature Stability of C@ZrSiO₄ Pigments

To evaluate practical performance, pigments synthesized under optimal conditions were incorporated into transparent glazes at 10 wt% loading and fired at

1200 ℃. Fig.7 shows SEM images, EDS elemental maps, and digital photographs of the glazed specimens. EDS mapping (Fig. 7b) confirms uniform dispersion of carbon within the $ZrSiO_4$ matrix (O, Si, Zr distribution). The glaze surface exhibits smooth morphology and consistent coloration (Fig. 7c), demonstrating the pigment's exceptional thermal stability. The retained seed-pulp structure after high-temperature firing underscores strong compatibility between the pigment and glaze matrix, ensuring superior chromatic performance.

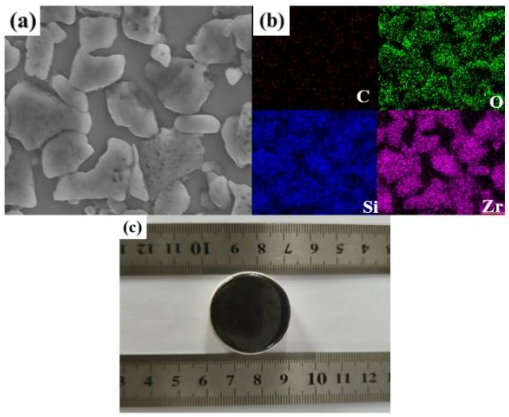

Fig. 7. C@ZrSiO4 pigment: SEM pattern (a); EDS-mapping photo (b)

3.5 Chromogenic Mechanism Analysis of C@$ZrSiO_4$ Pigments

To elucidate the chromogenic mechanism of C@$ZrSiO_4$ pigments synthesized via pressure field-assisted non-hydrolytic sol-gel (PFA-NHSG) methods, comparative FT-IR and SEM analyses were conducted between pigments prepared under optimal PFA-NHSG and conventional non-hydrolytic sol-gel (NHSG) conditions.

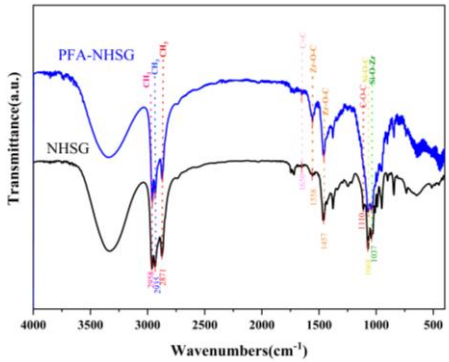

Fig. 8. FT-IR spectra of C@ZrSiO4 pigment prepared by PFA-NHSG methods

Fig. 8 presents the FT-IR spectra of PFA-NHSG-derived C@$ZrSiO_4$ pigments in the 400–2000 cm^{-1} range. Distinct vibrational absorption peaks are observed at 1037–1560 cm^{-1}, corresponding to Si–O–Zr [15], Si–O–C [17], and Zr–

O–C [18] bonds. Notably, the absence of the C–O–C [19] etherification peak at 1110 cm^{-1} (common in NHSG-derived samples) and the emergence of a C=C stretching vibration at 1650 cm^{-1} [20, 21] indicate structural reorganization of carbon-containing leaving groups under pressure fields. This reorganization promotes direct in situ carbonization, suppressing etherification and enhancing carbon yield. Furthermore, intensified residual absorption peaks for Zr–O–C, Si–O–C, and Si–O–Zr in PFA-NHSG spectra (Fig. 8) confirm that pressure fields not only accelerate $ZrSiO_4$ synthesis but also increase carbon functional group retention. The assignments of key infrared vibrations are summarized in Table 1.

Table 1

Bonding of infrared vibration peaks

Absorption peak position (cm-1)	Vibration mode	Reference
1037	Si-O-Zr	[15]
1068	Si-O-C	[17]
1460, 1558	Zr-O-C	[18]
1110	C–O–C	[19]
1650	C=C	[20],[21]

Fig. 9 displays TEM, EDS elemental mapping, and HR-TEM images of the optimized C@$ZrSiO_4$ pigment.

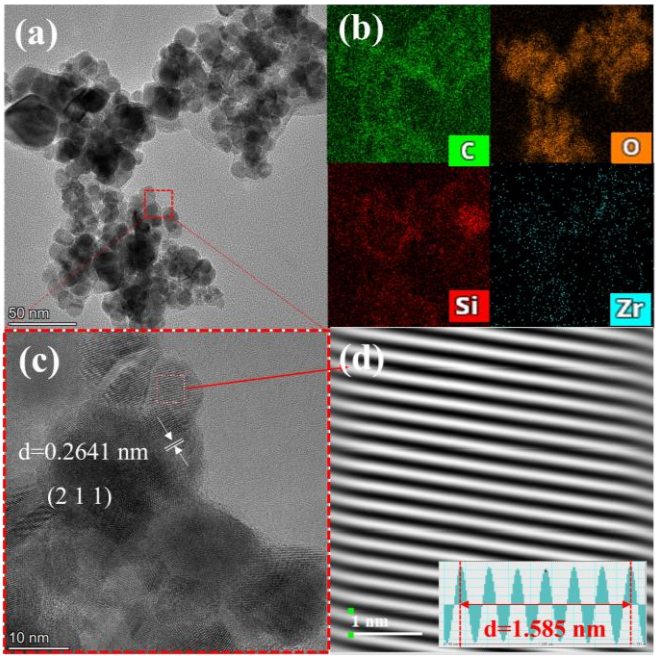

Fig. 9. C@ZrSiO4 pigment: TEM image (a); EDS area scanning (b); HR-TEM image (c); and a magnification of lattice fringes in selected areas (d)

Fig. 9(a) reveals a dense, pore-free $ZrSiO_4$ encapsulation layer embedding spherical carbon nanoparticles (~20 nm diameter). EDS mapping (Fig. 9(b) confirms homogeneous distribution of C, O, Si, and Zr within the composite. HR-TEM (Fig. 9(c)) resolves lattice fringes with a measured spacing of 2.64100 Å, corresponding to the (211) crystallographic plane of $ZrSiO_4$ (JCPDS #06-0266). Magnified lattice patterns (Fig. 9 (d)) corroborate the $ZrSiO_4$ shell structure. These findings validate a unique seed-pulp architecture, where uniformly dispersed in situ carbon nanoparticles are encapsulated within a high-density $ZrSiO_4$ matrix. Compared to conventional C@$ZrSiO_4$ pigments, this structure ensures enhanced chromaticity due to optimized carbon dispersion and encapsulation efficiency.

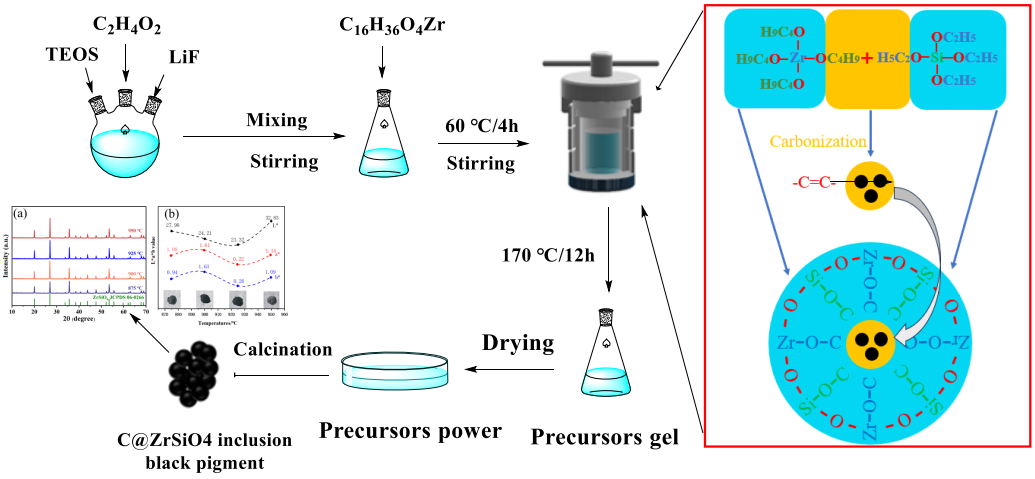

Fig. 10. Formation mechanism diagram of C@ZrSiO4 pigment

Fig. 10 illustrates the formation mechanism of C@$ZrSiO_4$ pigments via PFA-NHSG. The pressure field reduces activation energy for Si–O–Zr bond formation, significantly accelerating polycondensation. Concurrently, carbon-containing leaving groups undergo structural rearrangement, directly carbonizing into C=C bonds instead of participating in etherification. During calcination, residual Zr–O–C and Si–O–C bonds are fully carbonized, yielding a dense, homogeneous C@$ZrSiO_4$ composite. This dual effect of pressure—enhancing $ZrSiO_4$ crystallization and directing carbon precursor transformation—underpins the superior chromatic performance of the synthesized pigments.

4. Conclusions

To enhance the encapsulation efficiency of inclusions within $ZrSiO_4$-based pigments, this study employed zirconium butoxide as the zirconium source and carbon-containing organic functional groups in the precursor as the carbon source,

synthesizing C@$ZrSiO_4$ pigments with a novel seed-pulp structure via a pressure field-assisted non-hydrolytic sol-gel (PFA-NHSG) method. The effects of non-hydrolytic reaction temperature, pressure field treatment duration, and heat treatment parameters on the synthesis and encapsulation performance of C@$ZrSiO_4$ black pigments were systematically investigated, and the formation mechanism of the pigments was further elucidated. Optimal encapsulation was achieved under the following conditions: non-hydrolytic reaction temperature of 170 ℃, pressure field treatment duration of 12 h, calcination at 925 ℃ for 3.5 h, and subsequent oxidation at 700 ℃ for 2 h.

The best color rendering performance of C@ZrSiO4 black color was obtained (L*=19.03, a*=1.75, b*=1.84). The C@ZrSiO4 black color obtained under the optimal parameters is applied to the basic transparent glaze at 1200 ℃. The glaze surface is smooth and dark black (L*=22.03, a*=-0.39, b*=-0.56), which corresponds to the obvious improvement of the color rendering effect in the glaze.

The formation mechanism of C@$ZrSiO_4$ pigments was revealed: Under the pressure field, the non-hydrolytic polycondensation reaction is facilitated, promoting the formation of Si–O–Zr bonds. Simultaneously, carbon-containing groups undergo direct carbonization to form C=C bonds, bypassing intermediate etherification pathways. This structural reorganization of carbon precursors enables in situ carbon generation, which is uniformly embedded within the $ZrSiO_4$ matrix. Residual Zr–O–C and Si–O–C bonds in the precursor are fully carbonized during calcination, ultimately yielding a high-density C@$ZrSiO_4$ composite with enhanced chromatic properties. The synergistic effects of pressure field assistance—accelerating inorganic network formation and directing carbon precursor transformation—establish a robust foundation for designing eco-friendly, high-performance ceramic pigments.

Acknowledgement

This work was supported by the National Natural Science Foundation of China [grant numbers 52362041, 52262003]; Jiangxi Provincial Natural Science Foundation [grant numbers 20242BAB20166, 20232ACB204012, 20232BAB204031]; the Training Program for Academic and Technical Leaders of Major Disciplinesin Jiangxi Province [grant numbers 20243BCE51117]; the Jingdezhen Science and Technology plan project [grant numbers 20202GYZD013-14, 20212GYZD009-06, 20224GY008-07, 20224GY008-13].

REFERENCES

[1] *Enríquez E, Reinosa J J, Fuertes V*, et al. Advances and challenges of ceramic pigments for inkjet printing. Ceramics International, 2022, 48(21): 31080-31101.

[2] *Pfaff G*. Carbon black pigments. Physical Sciences Reviews, 2022, 7(2): 109-125.

[3] *He J, Jiang F, Yang S*, et al. Synthesis and coloring properties of a novel Na2NiMn2O6 black ceramic pigment. Ceramics International, 2025, 51(7): 9564-9569.
[4] *Li Z, Zhang X, Ma G*, et al. Effect of the Fe/Cr molar ratio and calcination temperature on the preparation of black ceramic pigment with stainless steel dust assisted by microwave processing. Journal of Cleaner Production, 2022, 372: 133751.
[5] *Dondi M, Zanelli C, Ardit M,* et al. Ni-free, black ceramic pigments based on Co—Cr—Fe—Mn spinels: A reappraisal of crystal structure, colour and technological behaviour. Ceramics International, 2013, 39(8): 9533-9547.
[6] *Maslennikova G N.* Pigments of the spinel type. Glass and ceramics, 2001, 58(5): 216-220.
[7] *Ozel E, Turan S*. Production and characterisation of iron-chromium pigments and their interactions with transparent glazes. Journal of the European Ceramic Society, 2003, 23(12): 2097-2104.
[8] *Zhao F, Li W, Luo H*. Sol–gel modified method for obtention of gray and pink ceramic pigments in zircon matrix. Journal of sol-gel science and technology, 2009, 49: 247-252.
[9] *Yekta B E, Tamizifar M, Rahimi N.* Synthesis of a zircon-cadmium sulfo selenide pigment by a sol-gel technique. Journal of the Ceramic Society of Japan, 2007, 115(1347): 757-760.
[10] *Ozel E, Turan S*. Production of coloured zircon pigments from zircon. Journal of the European Ceramic Society, 2007, 27(2-3): 1751-1757.
[11] *Zhang X J, Chen T, Jiang W H*, et al. Preparation and chromatic properties of encapsulated carbon black pigment via layer-by-layer self-assembly method. Advanced Materials Research, 2015, 1104: 15-20.
[12] *Chen T, Zhang X, Jiang W*, et al. Synthesis and application of C@ ZrSiO4 inclusion ceramic pigment from cotton cellulose as a colorant. Journal of the European Ceramic Society, 2016, 36(7): 1811-1820.
[13] *Tang H, Hu Q, Jiang W*, et al. Facile non-aqueous synthesis of high color rendering C@ ZrSiO4 encapsulation pigment with carbon-containing precursors as in-situ carbon sources. Ceramics International, 2018, 44(14): 16498-16506.
[14] *Jiang F, Li W, Wang T*, et al. Pressure field assisted non-hydrolytic sol-gel in-situ synthesis of novel seed-pulp-structured C@ ZrSiO4 pigments. Ceramics International, 2024, 50(15): 26343-26350.
[15] *Kongwudthiti S, Praserthdam P, Tanakulrungsank W*, et al. The influence of Si–O–Zr bonds on the crystal-growth inhibition of zirconia prepared by the glycothermal method. Journal of Materials Processing Technology, 2003, 136(1-3): 186-189.
[16] *Mori T, Yamamura H, Kobayashi H*, et al. Preparation of high-purity ZrSiO4 powder using sol–gel processing and mechanical properties of the sintered body. Journal of the American Ceramic Society, 1992, 75(9): 2420-2426.
[17] *Gao Y, Masuda Y, Yonezawa T*, et al. Site-selective deposition and micro-patterning of zirconia thin films on templates of self-assembled monolayers. Journal of the Ceramic Society of Japan, 2002, 110(5): 379-385.
[18] *Jung T H, Subramanian R V*. Alkali resistance enhancement of basalt fibers by hydrated zirconia films formed by the sol-gel process. Journal of materials research, 1994, 9(4): 1006-1013.
[19] *Gómez-Serrano V, Piriz-Almeida F, Durán-Valle C J,* et al. Formation of oxygen structures by air activation. A study by FT-IR spectroscopy. Carbon, 1999, 37(10): 1517-1528.
[20] *Guo Z, Huang H D, Nan D*, et al. Preparation and electrothermal performance of onion-like carbon/carbon nanofibre composite film. Chemical Physics Letters, 2023, 818: 140429.
[21] *Gohda S, Saito M, Yamada Y*, et al. Carbonization of phloroglucinol promoted by heteropoly acids. Journal of Materials Science, 2021, 56: 2944-2960.